Discrete unified gas kinetic scheme for all Knudsen number flows. III. Binary gas mixtures of Maxwell molecules

Yue Zhang,[1] Lianhua Zhu,[1] Ruijie Wang,[2] and Zhaoli Guo[1,*]

[1]*State Key Laboratory of Coal Combustion, School of Energy and Power Engineering, Huazhong University of Science and Technology, Wuhan 430074, China*

[2]*School of Power and Energy, Northwestern Polytechnical University, Xi'an 710072, China*

(Received 17 December 2017; published 14 May 2018)

Recently a discrete unified gas kinetic scheme (DUGKS) in a finite-volume formulation based on the Boltzmann model equation has been developed for gas flows in all flow regimes. The original DUGKS is designed for flows of single-species gases. In this work, we extend the DUGKS to flows of binary gas mixtures of Maxwell molecules based on the Andries-Aoki-Perthame kinetic model [P. Andries *et al.*, J. Stat. Phys. **106**, 993 (2002). A particular feature of the method is that the flux at each cell interface is evaluated based on the characteristic solution of the kinetic equation itself; thus the numerical dissipation is low in comparison with that using direct reconstruction. Furthermore, the implicit treatment of the collision term enables the time step to be free from the restriction of the relaxation time. Unlike the DUGKS for single-species flows, a nonlinear system must be solved to determine the interaction parameters appearing in the equilibrium distribution function, which can be obtained analytically for Maxwell molecules. Several tests are performed to validate the scheme, including the shock structure problem under different Mach numbers and molar concentrations, the channel flow driven by a small gradient of pressure, temperature, or concentration, the plane Couette flow, and the shear driven cavity flow under different mass ratios and molar concentrations. The results are compared with those from other reliable numerical methods. The results show that the proposed scheme is an effective and reliable method for binary gas mixtures in all flow regimes.

DOI: 10.1103/PhysRevE.97.053306

I. INTRODUCTION

Rarefied gas mixture flows exist widely in nature and practical applications, such as chemical reactions, evaporation-condensation, and the micro-electro-mechanical system (MEMS). The rarefaction degree of gas flows is normally characterized by the Knudsen number (Kn), which is defined as the ratio of the mean free path of gas molecules to the characteristic length of the system. The conventional fluid dynamics models, such as the Euler equations and the Navier-Stokes equations, are valid for continuum flows (Kn < 0.001), but for flows with relative large Kn, nonequilibrium effects will appear and continuum models become invalid [1].

Alternatively, the Boltzmann equation can be used to describe the gas mixture flows in all regimes. But it is difficult to obtain the accurate solutions of the Boltzmann equation directly due to the complicated collision term. Conventionally, the direct simulation Monte Carlo (DSMC) method was employed to investigate nonequilibrium behaviors of the rarefied gas mixtures in many studies, e.g., [2–5], which is a prevailing numerical technique for simulating moderate and highly rarefied gas flows. However, the streaming and collision processes of the DSMC are decoupled, such that the time step and mesh size are limited by the molecular collision time and the mean free path, respectively [6]. This limitation leads to expensive computational costs for continuum and near-continuum flows. It is noted that some efforts have been made to reduce these difficulties [7,8]. Besides the DSMC method, some deterministic numerical methods for the Boltzmann equation, such as [9–12], have been applied to gas mixture flows with simple geometries. These deterministic methods can offer accurate solutions of the full Boltzmann equation, but are usually rather complicated and computationally expensive.

Some efforts have been devoted to simplify the full Boltzmann equation for gas mixtures by replacing the full collision operator with certain simplified models. Compared with the single-species kinetic model equations, the nonunitary mass ratio between different molecular species increases the difficulty. One of such models is the McCormack model [13] which linearizes the nonlinear collision term under the assumption that the systems only slightly deviate from equilibrium; it is noted that extension to nonlinear problems has also been made recently [14,15]. Another simplified model is the so called Andries-Aoki-Perthame (AAP) model [16] in which the collision term is modeled by a single Bhatnagar-Gross-Krook (BGK) [17] operator considering both self-collision and cross-collision effects. Owing to its simple formulation, the AAP model has been applied to a number of rarefied mixture flows [18–21].

Based on the kinetic models, some numerical schemes have been developed, such as the lattice Boltzmann method (LBM) [22–24] and the discrete velocity method (DVM) [25–27]. Particularly, a unified gas kinetic scheme (UGKS) for binary gas mixtures of hard sphere molecules and Maxwell molecules has been constructed [28,29] for all flow regimes based on the AAP model. The original UGKS is designed for single-species gas flows covering different flow regimes [30,31], which is

*Corresponding author: zlguo@hust.edu.cn

a finite-volume scheme for the discrete velocity Boltzmann model equation. A distinctive feature of the UGKS is that the reconstruction of the numerical flux is based on the local analytical characteristic solution of the kinetic equation rather than interpolation, such that the numerical dissipation is small. Furthermore, the semi-implicit discretization of the collision term in the UGKS enables it to be uniformly stable, i.e., the time step is not limited by the mean collision time. The UGKS also has the nice asymptotic preserving (AP) property [32], i.e., it solves the Navier-Stokes equations in the continuum flow regime.

Recently, another unified kinetic method, i.e., the discrete unified gas kinetic scheme (DUGKS) [33,34], was developed for single-species gas flows covering different flow regimes. The DUGKS shares all the advantages of the UGKS, but some apparent differences also exist between the two schemes. First, they achieve the characteristic solution by different approaches: the UGKS uses an analytical temporal-spatial integral solution of the governing equation, while the DUGKS uses a discrete characteristic solution which is much simpler than the analytical integral one. Second, in the UGKS, flow variables are required to be updated first to evaluate explicitly the implicit treatment of the collision term, while the DUGKS removes the implicitness by introducing a new distribution function that is tracked in implementation. The above differences make the DUGKS more efficient than the UGKS [28]. Compared with the LBM, the computational cost of the DUGKS is somewhat expensive with the same uniform mesh, but is less expensive if a nonuniform mesh is employed [35]. The DUGKS has already been applied successfully to flows of single-species gases from continuum to rarefied regimes [36–39]. Recently, some extensions of DUGKS to complex flows have also been made. For example, a DUGKS for two-phase flows was proposed based on the phase-field theory [40]. Another possible extension is for flows in porous media, by making use of unstructured meshes like the finite-volume LBM [41,42].

The aim of this work is to extend the DUGKS to binary gas mixtures of Maxwell molecules based on the AAP model. The remaining part of this paper is organized as follows. Section II will introduce the AAP model for binary gas mixtures. In Sec. III, the DUGKS will be constructed based on the AAP model, and in Sec. IV several numerical tests are performed. Finally, a brief summary is given in Sec. V.

II. THE AAP MODEL FOR GAS MIXTURES

The Boltzmann equation for a binary gas mixture of species A and B can be written as [43]

$$\frac{\partial f_\alpha}{\partial t} + \boldsymbol{\xi}\cdot\nabla f_\alpha = Q_\alpha(f,f), \tag{1}$$

with

$$\begin{aligned} Q_\alpha(f,f) &= \sum_{\alpha=A,B} Q_{\alpha\beta}(f_\alpha,f_\beta), \quad Q_{\alpha\beta}(f_\alpha,f_\beta) \\ &= \int_{R^3}\int_{B_+} (f'_\alpha f'_{\beta^*} - f_\alpha f_{\beta^*}) B_{\alpha\beta}(\boldsymbol{N}\cdot\boldsymbol{V},|\boldsymbol{V}|) \\ &\quad \times d\boldsymbol{\xi}_* d\boldsymbol{N}, \end{aligned} \tag{2}$$

where the Greek letters α and β will be used symbolically to represent the gas species, i.e., $\{\alpha,\beta\} = \{A,B\}$; $f_\alpha \equiv f_\alpha(\boldsymbol{x},\boldsymbol{\xi},t)$ represents the distribution function of species α with particle velocity $\boldsymbol{\xi}$ at position $\boldsymbol{x}$ and time t in 3-dimensional physical space; $Q_\alpha(f,f)$ is the Boltzmann collision operator for species α, $B_{\alpha\beta}(\boldsymbol{N}\cdot\boldsymbol{V},|\boldsymbol{V}|)$ is the collision kernel which is decided by the intermolecular force between species α and β, $\boldsymbol{\xi}$ and $\boldsymbol{\xi}_*$ are precollision velocities, $\boldsymbol{N}$ is a unit vector, and B_+ is the semisphere defined by $\boldsymbol{N}\cdot\boldsymbol{V} = 0$, where $\boldsymbol{V}$ is the relative velocity

$$\boldsymbol{V} = \boldsymbol{\xi} - \boldsymbol{\xi}_*. \tag{3}$$

From conservation laws of momentum and energy,

$$\begin{aligned} m_\alpha\boldsymbol{\xi} + m_\beta\boldsymbol{\xi}_* &= m_\alpha\boldsymbol{\xi}' + m_\beta\boldsymbol{\xi}'_*, \\ m_\alpha|\xi|^2 + m_\beta|\xi_*|^2 &= m_\alpha|\xi'|^2 + m_{|}\xi'_*|^2, \end{aligned} \tag{4}$$

the postcollision velocities $\boldsymbol{\xi}'$ and $\boldsymbol{\xi}'_*$ can be written as

$$\begin{aligned} \boldsymbol{\xi}' &= \boldsymbol{\xi} - \frac{2m_{\alpha\beta}}{m_\alpha}\boldsymbol{N}[(\boldsymbol{\xi}-\boldsymbol{\xi}_*)\cdot\boldsymbol{N}], \\ \boldsymbol{\xi}'_* &= \boldsymbol{\xi}_* + \frac{2m_{\alpha\beta}}{m_\beta}\boldsymbol{N}[(\boldsymbol{\xi}-\boldsymbol{\xi}_*)\cdot\boldsymbol{N}], \end{aligned} \tag{5}$$

with the reduced mass being

$$m_{\alpha\beta} = \frac{m_\alpha m_\beta}{(m_\alpha + m_\beta)}, \tag{6}$$

in which m_α and m_β are the molecular masses of species α and β, respectively. Without loss of generality, we assume $m_A < m_B$.

Furthermore, the macroscopic quantities of species α, such as the molecular number density n_α, mass density ρ_α, flow velocity $\boldsymbol{u}_\alpha$, total energy E_α, and internal energy ϵ_α are calculated as the moments of distribution function f_α:

$$\rho_\alpha = \int f_\alpha d\boldsymbol{\xi}, \quad n_\alpha = \rho_\alpha/m_\alpha, \tag{7a}$$

$$\rho_\alpha\boldsymbol{u}_\alpha = \int \boldsymbol{\xi} f_\alpha d\boldsymbol{\xi}, \tag{7b}$$

$$\rho_\alpha E_\alpha = \frac{1}{2}\int \xi^2 f_\alpha d\boldsymbol{\xi} = \frac{1}{2}\rho_\alpha u_\alpha^2 + \epsilon_\alpha, \tag{7c}$$

$$\epsilon_\alpha = \frac{1}{2}\int |\boldsymbol{c}_\alpha|^2 f_\alpha d\boldsymbol{\xi}, \tag{7d}$$

where $\boldsymbol{c}_\alpha = \boldsymbol{\xi} - \boldsymbol{u}_\alpha$. The mass density ρ_m, number density n_m, flow velocity $\boldsymbol{u}_m$, energy E_m, and internal energy ϵ_m of the mixture can then be obtained as

$$\rho_m = \sum_{\alpha=A,B}\rho_\alpha, \quad n_m = \sum_{\alpha=A,B} n_\alpha, \tag{8a}$$

$$\rho_m\boldsymbol{u}_m = \sum_{\alpha=A,B}\rho_\alpha\boldsymbol{u}_\alpha, \tag{8b}$$

$$\rho_m E_m = \sum_{\alpha=A,B}\rho_\alpha E_\alpha = \frac{1}{2}\rho_m|u_m|^2 + \epsilon_m. \tag{8c}$$

The AAP model is a relaxation approximation of the full Boltzmann equation in Eq. (1),

$$\frac{\partial f_\alpha}{\partial t} + \boldsymbol{\xi}\cdot\nabla f_\alpha = \Omega_\alpha(f,f) = \frac{f_\alpha^* - f_\alpha}{\tau_\alpha}, \tag{9}$$

where $\alpha = A$ or B with

$$f_\alpha^* = \rho_\alpha\left(\frac{m_\alpha}{2\pi k_B T_\alpha^*}\right)^{\frac{3}{2}} \exp\left[-\frac{m_\alpha}{2k_B T_\alpha^*}(\boldsymbol{\xi} - \boldsymbol{u}_\alpha^*)^2\right], \tag{10}$$

in which k_B is the Boltzmann constant. The parameters $\boldsymbol{u}_\alpha^*$ and T_α^* are introduced to recover the correct interspecies transfer of momentum and energy due to the collisions between molecules of different species [16],

$$\boldsymbol{u}_\alpha^* = \boldsymbol{u}_\alpha + \tau_\alpha \sum_{\beta=A,B} 2\frac{\rho_\beta}{m_\alpha + m_\beta}\theta_{\alpha\beta}(\boldsymbol{u}_\beta - \boldsymbol{u}_\alpha), \tag{11a}$$

$$\begin{aligned}\frac{3}{2}k_B T_\alpha^* = {}& \frac{3}{2}k_B T_\alpha - \frac{m_\alpha}{2}(\boldsymbol{u}_\alpha^* - \boldsymbol{u}_\alpha)^2 \\ & + \tau_\alpha \sum_{\beta=A,B} 4m_\alpha \frac{\rho_\beta}{(m_\alpha + m_\beta)^2}\theta_{\alpha\beta} \\ & \times\left[\frac{3}{2}k_B T_\beta - \frac{3}{2}k_B T_\alpha + \frac{m_\beta}{2}(\boldsymbol{u}_\beta - \boldsymbol{u}_\alpha)^2\right],\end{aligned} \tag{11b}$$

with $\theta_{\alpha\beta}$ being the interaction coefficient between molecules. The mean collision time and frequency from the AAP model can be expressed as

$$\nu_\alpha = \frac{1}{\tau_\alpha} = \chi \sum_{\beta=A,B} \frac{\theta_{\alpha\beta}\rho_\beta}{m_\beta}, \tag{12}$$

where χ is either 1 or selected to make τ_α be the same with that of the single-species gas when all species are equal. In this paper, we fix $\chi = 1$. The interaction coefficient $\theta_{\alpha\beta}$ is related to the molecular interaction model. For example, for Maxwell molecules [44],

$$\theta_{\alpha\beta} = 0.422\pi\left[\frac{a_{\alpha\beta}(m_\alpha + m_\beta)}{m_\alpha m_\beta}\right]^{\frac{1}{2}}, \tag{13}$$

where $a_{\alpha\beta}$ is the constant of proportionality, i.e.,

$$U_{\alpha\beta} = \frac{a_{\alpha\beta}}{4r^4}, \tag{14}$$

where $U_{\alpha\beta}$ is the potential between two molecules of masses m_α and m_β with a distance r.

In this work, we will consider Maxwell molecules and the force constant ratios a_{BB}/a_{AA} and a_{AB}/a_{AA} should be known. According to the viscosity of the mixture given by the AAP model [16]

$$\mu = k_B T_0 \sum_{\alpha=A,B} \frac{n_\alpha}{\nu_\alpha}, \tag{15}$$

if we take $n_\alpha = 0$ then the binary gas mixture reduces to a single gas of species β and its viscosity is

$$\mu_\beta = k_B T_0 \frac{n_\beta}{\nu_\beta} = k_B T_0 \frac{1}{\theta_{\beta\beta}}. \tag{16}$$

Then, based on Eq. (13), we can obtain

$$\frac{a_{\beta\beta}}{a_{\alpha\alpha}} = \left(\frac{\mu_\alpha}{\mu_\beta}\right)^2 \frac{m_\beta}{m_\alpha}. \tag{17}$$

The constant $a_{\alpha\beta}$ can then be determined as [13]

$$a_{\alpha\beta} = \sqrt{a_{\alpha\alpha}a_{\beta\beta}}. \tag{18}$$

III. DISCRETE UNIFIED GAS KINETIC SCHEME

A. Updating of the cell-averaged distribution function

For problems of $D < 3$ dimensional, the kinetic equation (9) can be simplified by introducing a reduced one. Specially, the original distribution function f_α can be expressed as $f_\alpha = f_\alpha(\boldsymbol{x},\boldsymbol{\xi},\boldsymbol{\eta},t)$, where $\boldsymbol{\xi} = (\xi_1,\ldots,\xi_D)$, $\boldsymbol{x} = (x_1,\ldots,x_D)$, and $\boldsymbol{\eta} = (\xi_{D+1},\ldots,\xi_3)$ is a vector of length $L = 3 - D$, consisting of the rest components of the three-dimensional (3D) velocity space (ξ_1,ξ_2,ξ_3). Since the evolution of the distribution function f_α is only relevant to the D-dimensional velocity and independent of $\boldsymbol{\eta}$, a reduced distribution function is used to remove the dependence of the redundant variable $\boldsymbol{\eta}$ [45,46],

$$g_\alpha(\boldsymbol{x},\boldsymbol{\xi},t) = \int f_\alpha(\boldsymbol{x},\boldsymbol{\xi},\boldsymbol{\eta},t)d\boldsymbol{\eta}. \tag{19}$$

However, the energy defined by Eq. (7) cannot be determined by this g_α solely, and another reduced distribution function is required,

$$h_\alpha(\boldsymbol{x},\boldsymbol{\xi},t) = \int \eta^2 f_\alpha(\boldsymbol{x},\boldsymbol{\xi},\boldsymbol{\eta},t)d\boldsymbol{\eta}. \tag{20}$$

The macroscopic flow variables of species α can be computed from the two reduced distribution functions as

$$\begin{aligned}\rho_\alpha &= \int g_\alpha d\boldsymbol{\xi}, \quad \rho_\alpha \boldsymbol{u}_\alpha = \int \boldsymbol{\xi} g_\alpha d\boldsymbol{\xi}, \\ \rho_\alpha E_\alpha &= \frac{1}{2}\int (\xi^2 g_\alpha + h_\alpha)d\boldsymbol{\xi},\end{aligned} \tag{21}$$

and the heat flux $\boldsymbol{q}_\alpha$ and stress tensor $\boldsymbol{P}_\alpha$ can be computed as

$$\boldsymbol{q}_\alpha = \frac{1}{2}\int \boldsymbol{c}_\alpha\left(c_\alpha^2 g_\alpha + h_\alpha\right)d\boldsymbol{\xi}, \quad \boldsymbol{P}_\alpha = \int \boldsymbol{c}_\alpha\boldsymbol{c}_\alpha\left(g_\alpha - g_\alpha^{eq}\right)d\boldsymbol{\xi}, \tag{22}$$

where

$$g_\alpha^{\mathrm{eq}} = \rho_\alpha\left(\frac{m_\alpha}{2\pi k_B T_\alpha}\right)^{D/2} \exp\left[-\frac{m_\alpha}{2k_B T_\alpha}(\boldsymbol{\xi} - \boldsymbol{u}_\alpha)^2\right]. \tag{23}$$

Note that g_α^{eq} cannot give any communication among species in the multispecies system.

The evolution equations for g_α and h_α can be deduced from Eq. (9),

$$\frac{\partial g_\alpha}{\partial t} + \boldsymbol{\xi}\cdot\nabla g_\alpha = \Omega(g_\alpha) \equiv \frac{g_\alpha^* - g_\alpha}{\tau_\alpha}, \tag{24a}$$

$$\frac{\partial h_\alpha}{\partial t} + \boldsymbol{\xi}\cdot\nabla h_\alpha = \Omega(h_\alpha) \equiv \frac{h_\alpha^* - h_\alpha}{\tau_\alpha}, \tag{24b}$$

where

$$g_\alpha^* = \rho_\alpha\left(\frac{m_\alpha}{2\pi k_B T_\alpha^*}\right)^{D/2}\exp\left[-\frac{m_\alpha}{2k_B T_\alpha^*}(\boldsymbol{\xi}-\boldsymbol{u}_\alpha^*)^2\right], \quad (25a)$$

$$h_\alpha^* = (3-D)R_\alpha T_\alpha^* g_\alpha^*, \quad (25b)$$

with $R_\alpha = k_B/m_\alpha$.

Then the DUGKS for a binary gas mixture is constructed based on Eq. (24), which can be rewritten as

$$\frac{\partial \phi_\alpha}{\partial t} + \boldsymbol{\xi}\cdot\nabla\phi_\alpha = \Omega_\alpha \equiv \frac{\phi_\alpha^* - \phi_\alpha}{\tau_\alpha}, \quad (26)$$

where $\phi_\alpha = g_\alpha$ or h_α, $\phi_\alpha^* = g_\alpha^*$ or h_α^*. As a finite volume scheme, the computation domain is first divided into a set of control volumes (cells). Then integrating Eq. (26) over a control volume V_j centered at $\boldsymbol{x}_j$ from time t_n to t_{n+1}, and employing the midpoint rule for the time integration of the convective term and trapezoidal rule for the collision term inside each cell, the evolution equation for species α can be written as

$$\phi_{\alpha,j}^{n+1}(\boldsymbol{\xi}) - \phi_{\alpha,j}^{n}(\boldsymbol{\xi}) = -\frac{\Delta t}{|V_j|}\mathcal{F}_{\alpha,j}^{n+1/2}(\boldsymbol{\xi}) + \frac{\Delta t}{2}\left[\Omega_{\alpha,j}^{n}(\boldsymbol{\xi}) + \Omega_{\alpha,j}^{n+1}(\boldsymbol{\xi})\right]. \quad (27)$$

Here $\Delta t = t_{n+1} - t_n$ is the time step, $|V_j|$ is the volume of the cell V_j, and $\phi_{\alpha,j}^n$ and $\Omega_{\alpha,j}^n$ are the cell averaged values of ϕ_α and Ω_α defined by

$$\phi_{\alpha,j}^{n}(\boldsymbol{\xi}) = \frac{1}{|V_j|}\int_{V_j}\phi_\alpha(\boldsymbol{x},\boldsymbol{\xi},t_n)d\boldsymbol{x}, \quad (28a)$$

$$\Omega_{\alpha,j}^{n}(\boldsymbol{\xi}) = \frac{1}{|V_j|}\int_{V_j}\Omega_\alpha(\boldsymbol{x},\boldsymbol{\xi},t_n)d\boldsymbol{x}. \quad (28b)$$

The term $\mathcal{F}_{\alpha,j}^{n+1/2}$ in Eq. (27) is the distribution function flux across the cell interface,

$$\mathcal{F}_{\alpha,j}^{n+1/2}(\boldsymbol{\xi}) = \int_{\partial V_j}(\boldsymbol{\xi}\cdot\boldsymbol{n})\phi_\alpha(\boldsymbol{x},\boldsymbol{\xi},t_{n+1/2})d\boldsymbol{S}, \quad (29)$$

where $\boldsymbol{n}$ is the outward unit vector normal to the cell surface ∂V_j. It is clear that the updating rule given by Eq. (27) is implicit due to the term $\Omega_{\alpha,j}^{n+1}$. In order to obtain an explicit form, two new distribution functions are introduced,

$$\tilde{\phi}_\alpha = \phi_\alpha - \frac{\Delta t}{2}\Omega_\alpha = \frac{2\tau_\alpha+\Delta t}{2\tau_\alpha}\phi_\alpha - \frac{\Delta t}{2\tau_\alpha}\phi_\alpha^*, \quad (30a)$$

$$\tilde{\phi}_\alpha^+ = \phi_\alpha + \frac{\Delta t}{2}\Omega_\alpha = \frac{2\tau_\alpha-\Delta t}{2\tau_\alpha+\Delta t}\phi_\alpha + \frac{2\Delta t}{2\tau_\alpha+\Delta t}\phi_\alpha^*. \quad (30b)$$

Then Eq. (27) can be rewritten as

$$\tilde{\phi}_{\alpha,j}^{n+1} = \tilde{\phi}_{\alpha,j}^{+,n} - \frac{\Delta t}{|V_j|}\mathcal{F}_{\alpha,j}^{n+1/2}. \quad (31)$$

To avoid the implicity of Eq. (27), we can track the evolution of $\tilde{\phi}_\alpha$ instead of the original distribution function ϕ_α.

Note that the moments of $\tilde{g}_\alpha$ and $\tilde{h}_\alpha$ have the following expressions:

$$\int \tilde{g}_\alpha d\boldsymbol{\xi} = \rho_\alpha, \quad (32a)$$

$$\int \boldsymbol{\xi}\tilde{g}_\alpha d\boldsymbol{\xi} = \frac{2\tau_\alpha+\Delta t}{2\tau_\alpha}\int \boldsymbol{\xi} g_\alpha d\boldsymbol{\xi} - \frac{\Delta t}{2\tau_\alpha}\int \boldsymbol{\xi} g_\alpha^* d\boldsymbol{\xi} = \frac{2\tau_\alpha+\Delta t}{2\tau_\alpha}\rho_\alpha\boldsymbol{u}_\alpha - \frac{\Delta t}{2\tau_\alpha}\rho_\alpha\boldsymbol{u}_\alpha^*, \quad (32b)$$

$$\frac{1}{2}\int(\xi^2\tilde{g}_\alpha + \tilde{h}_\alpha)d\boldsymbol{\xi} = \frac{2\tau_\alpha+\Delta t}{2\tau_\alpha}\int\frac{1}{2}(\xi^2 g_\alpha + h_\alpha)d\boldsymbol{\xi} - \frac{\Delta t}{2\tau_\alpha}\int\frac{1}{2}(\xi^2 g_\alpha^* + h_\alpha^*)d\boldsymbol{\xi} = \frac{2\tau_\alpha+\Delta t}{2\tau_\alpha}\rho_\alpha E_\alpha - \frac{\Delta t}{2\tau_\alpha}\rho_\alpha E_\alpha^*, \quad (32c)$$

where $\rho_\alpha E_\alpha^* = \rho_\alpha u_\alpha^{*2}/2 + \rho_\alpha R_\alpha T_\alpha^*/(\gamma-1)$ with γ being the the specific heat ratio. Once the distribution functions $\tilde{g}_\alpha$ and $\tilde{h}_\alpha$ are known, the macroscopic variables $\boldsymbol{W}_\alpha = (\rho_\alpha, \rho_\alpha\boldsymbol{u}_\alpha, \rho_\alpha E_\alpha)$ and $\boldsymbol{W}_\alpha^* = (\rho_\alpha, \rho_\alpha\boldsymbol{u}_\alpha^*, \rho_\alpha E_\alpha^*)$ can be solved from the moments of them according to Eq. (32). Then Eq. (32) becomes an equation set with four relations [Eq. (32b) and Eq. (32c) for $\alpha = A, B$] and eight unknown variables ($\boldsymbol{u}_\alpha, T_\alpha, \boldsymbol{u}_\alpha^*$, and T_α^* for $\alpha = A, B$). To ensure the equation set is closed, the exchange relations between species A and B in Eq. (11) are introduced. Then the macroscopic quantities $\boldsymbol{u}_\alpha, T_\alpha, \boldsymbol{u}_\alpha^*$, and T_α^* for each species can be solved from Eqs. (32) and (11). In particular, for Maxwell molecules, the interaction coefficients $\theta_{\alpha\beta}$ and $\theta_{\alpha\alpha}$ only depend on the mass ratio [see Eq. (13)]. By this way, the macroscopic variables $\boldsymbol{W}_\alpha$ and $\boldsymbol{W}_\alpha^*$ for each species can be expressed in terms of the moments of $\tilde{g}_\alpha$ and $\tilde{h}_\alpha$ explicitly.

B. Flux evaluation

To update $\tilde{\phi}_{\alpha,j}^{n+1}$ according to Eq. (31), the flux $\mathcal{F}^{n+1/2}$ should be evaluated. Based on the definition of flux in Eq. (29), $\mathcal{F}^{n+1/2}$ can be calculated by reconstructing the distribution function $\phi_\alpha(\boldsymbol{x},\boldsymbol{\xi},t_{n+1/2})$ at the cell interface. To this end, Eq. (26) is integrated along the characteristic line from time t_n to $t_{n+1/2}$,

$$\phi_\alpha(\boldsymbol{x}_b,\boldsymbol{\xi},t_n+s) - \phi_\alpha(\boldsymbol{x}_b-\boldsymbol{\xi}s,\boldsymbol{\xi},t_n) = \frac{s}{2}\left[\Omega_\alpha(\boldsymbol{x}_b,\boldsymbol{\xi},t_n+s) + \Omega_\alpha(\boldsymbol{x}_b-\boldsymbol{\xi}s,\boldsymbol{\xi},t_n)\right], \quad (33)$$

where $s = \Delta t/2$ and $\boldsymbol{x}_b$ is the interface center of cell j, and the trapezoidal rule is applied to evaluate the collision term again. In order to remove the implicity caused by the term $\Omega_\alpha^{n+1/2}$, another two auxiliary distribution functions are introduced,

$$\bar{\phi}_\alpha = \phi_\alpha - \frac{s}{2}\Omega_\alpha = \frac{2\tau_\alpha+s}{2\tau_\alpha}\phi_\alpha - \frac{s}{2\tau_\alpha}\phi_\alpha^*, \quad (34a)$$

$$\bar{\phi}_\alpha^+ = \phi_\alpha + \frac{s}{2}\Omega_\alpha = \frac{2\tau_\alpha-s}{2\tau_\alpha+s}\phi_\alpha + \frac{2s}{2\tau_\alpha+s}\phi_\alpha^*. \quad (34b)$$

Then Eq. (33) can be rewritten as

$$\bar{\phi}_\alpha(\boldsymbol{x}_b,\boldsymbol{\xi},t_{n+1/2}) = \bar{\phi}_\alpha^+(\boldsymbol{x}_b-\boldsymbol{\xi}s,\boldsymbol{\xi},t_n), \quad (35)$$

where

$$\bar{\phi}_\alpha^+(\boldsymbol{x}_b-\boldsymbol{\xi}s,\boldsymbol{\xi},t_n)=\bar{\phi}_\alpha^+(\boldsymbol{x}_j,\boldsymbol{\xi},t_n)+(\boldsymbol{x}_b-\boldsymbol{x}_j-\boldsymbol{\xi}s)\cdot\boldsymbol{\delta}_j,\quad(\boldsymbol{x}_b-\boldsymbol{\xi}s)\in V_j. \tag{36}$$

Here $\boldsymbol{\delta}_j$ is the slope of $\bar{\phi}_\alpha^+$ in cell j. For example, in the one-dimensional (1D) case, the distribution function ϕ_α at the cell interface $x_b=x_{j+1/2}$ is reconstructed through approximating the distribution function $\bar{\phi}_\alpha^+$ as

$$\bar{\phi}_\alpha^+(x_b-\xi s,\xi,t_n)=\begin{cases}\bar{\phi}_\alpha^+(x_j,\xi,t_n)+(x_b-x_j-\xi s)\cdot\delta_j, & \xi>0,\\ \bar{\phi}_\alpha^+(x_{j+1},\xi,t_n)+(x_b-x_{j+1}-\xi s)\cdot\delta_j, & \xi<0.\end{cases} \tag{37}$$

Here the van Leer limiter [47] is applied to determine the slope $\boldsymbol{\delta}_j$ for discontinuous problems. Once the distribution function $\bar{\phi}_\alpha$ at the interface is known, the original distribution function ϕ_α can be obtained according to Eq. (34), i.e.,

$$\phi_\alpha(\boldsymbol{x}_b,\boldsymbol{\xi},t_{n+1/2})=\frac{2\tau_\alpha}{2\tau_\alpha+s}\bar{\phi}_\alpha(\boldsymbol{x}_b,\boldsymbol{\xi},t_n+s)+\frac{s}{2\tau_\alpha+s}\phi_\alpha^*(\boldsymbol{x}_b,\boldsymbol{\xi},t_n+s). \tag{38}$$

Note that the macroscopic variables used to evaluate the distribution function ϕ_α^* are computed from $\bar{\phi}_\alpha$ directly as

$$\int\bar{g}_\alpha d\boldsymbol{\xi}=\rho_\alpha, \tag{39a}$$

$$\int\boldsymbol{\xi}\bar{g}_\alpha d\boldsymbol{\xi}=\frac{2\tau_\alpha+s}{2\tau_\alpha}\int\boldsymbol{\xi}g_\alpha d\boldsymbol{\xi}-\frac{s}{2\tau_\alpha}\int\boldsymbol{\xi}g_\alpha^* d\boldsymbol{\xi}=\frac{2\tau_\alpha+s}{2\tau_\alpha}\rho_\alpha\boldsymbol{u}_\alpha-\frac{s}{2\tau_\alpha}\rho_\alpha\boldsymbol{u}_\alpha^*, \tag{39b}$$

$$\frac{1}{2}\int(\xi^2\bar{g}_\alpha+\bar{h}_\alpha)d\boldsymbol{\xi}=\frac{2\tau_\alpha+s}{2\tau_\alpha}\int\frac{1}{2}(\xi^2g_\alpha+h_\alpha)d\boldsymbol{\xi}-\frac{s}{2\tau_\alpha}\int\frac{1}{2}(\xi^2g_\alpha^*+h_\alpha^*)d\boldsymbol{\xi}=\frac{2\tau_\alpha+s}{2\tau_\alpha}\rho_\alpha E_\alpha-\frac{s}{2\tau_\alpha}\rho_\alpha E_\alpha^*. \tag{39c}$$

Similarly to the previous treatment of cell averaged macroscopic variables, Eqs. (39) and (11) constitute a closed system for eight unknown variables ($\boldsymbol{u}_\alpha, T_\alpha, \boldsymbol{u}_\alpha^*$, and T_α^* at cell interface $\boldsymbol{x}_b$ and half time step $t_{n+1/2}$ for each species α). These macroscopic variables can also be obtained explicitly, and the original distribution function ϕ_α can be updated from Eq. (38). Then the flux across each cell interface can be computed according to Eq. (29). Finally, the cell averaged distribution function $\tilde{\phi}_\alpha$ in each cell is updated from t_n to t_{n+1} according to Eq. (31).

In practical implementation, the velocity space is discretized into a set of discrete velocities $\boldsymbol{\xi}_i(i=1,2,\ldots,b)$. Certain quadrature rules, such as the Gaussian-Hermite or Newton-Cotes formula, can be chosen to discretize the velocity space and approximate the moments, e.g.,

$$\rho_\alpha=\sum_i w_i\tilde{g}_\alpha(\boldsymbol{\xi}_i),\quad \rho_\alpha\boldsymbol{u}_\alpha=\sum_i w_i\boldsymbol{\xi}_i\tilde{g}_\alpha(\boldsymbol{\xi}_i),$$
$$\rho_\alpha E_\alpha=\frac{1}{2}\sum_i w_i\left[\xi_i^2\tilde{g}_\alpha(\boldsymbol{\xi}_i)+\tilde{h}_\alpha(\boldsymbol{\xi}_i)\right], \tag{40}$$

where w_i are the quadrature weights.

The time step in DUGKS is determined by the Courant-Friedrichs-Lewy (CFL) condition,

$$\Delta t=\varsigma\frac{\Delta x}{U_m+\xi_m}, \tag{41}$$

where $0<\varsigma<1$ is the CFL number, Δx is the minimal mesh size, ξ_m is the maximum discrete velocity, and U_m is the maximum flow velocity. Due to the coupling of particle transport and collision in the reconstruction of the interface distribution function, the DUGKS has the asymptotic preserving (AP) property [30,32]. As a result, the time step Δt is not limited by the particle collision time but determined by the CFL number, and the DUGKS is uniformly stable with respect to the Knudsen number.

C. Algorithm

Now we list the computational procedure of the DUGKS for a binary gas mixture made up of Maxwell molecules from t_n to t_{n+1}:

(1) Calculate $\tilde{\phi}_\alpha^{+,n}$ and $\bar{\phi}_\alpha^{+,n}$ at each cell center according to Eqs. (30) and (34), respectively.

(2) Reconstruct the distribution function $\bar{\phi}_\alpha^+(\boldsymbol{x}_b-\boldsymbol{\xi}s,\boldsymbol{\xi},t_n)$ according to Eq. (36).

(3) Calculate the distribution function $\bar{\phi}_\alpha(\boldsymbol{x}_b,\boldsymbol{\xi},t_{n+1/2})$ according to Eq. (35).

(4) Calculate the macroscopic variables $\boldsymbol{W}_\alpha(\boldsymbol{x}_b,t_{n+1/2})$ and $\boldsymbol{W}_\alpha^*(\boldsymbol{x}_b,t_{n+1/2})$ according to Eqs. (39) and (11).

(5) Calculate the original distribution function at each cell interface $\phi_\alpha(\boldsymbol{x}_b,\boldsymbol{\xi},t_{n+1/2})$ according to Eq. (38).

(6) Calculate the microflux $\mathcal{F}^{n+1/2}$ across each cell interface from $\phi_\alpha(\boldsymbol{x}_b,\boldsymbol{\xi},t_{n+1/2})$ according to Eq. (29).

(7) Update the cell averaged distribution function $\tilde{\phi}_\alpha$ in each cell according to Eq. (31).

IV. NUMERICAL EXAMPLES

In this section, the proposed DUGKS will be validated by several test cases, including the shock structure problem under different Mach numbers, the channel flow driven by small pressure gradient, or temperature gradient or concentration gradient, and the $1D$ and $2D$ shear driven flows over a wide range of Knudsen numbers. In each test different mass ratios and molar concentrations will be considered.

A. Shock structure

The first test case is the shock structure for a binary gas mixture. Consider a normal shock formed by a mixture made up of a light species (A) and a heavy species (B). The molar concentrations, number densities, velocities, and temperatures are expressed as $\chi_1^{A,B}, n_1^{A,B}, U_1, T_1$ in the upstream and $\chi_2^{A,B}$, $n_1^{A,B}$, U_2, T_2 in the downstream, where $\chi^{A,B}=n^{A,B}/(n^A+n^B)$. The Mach number is defined as

$$\mathrm{Ma}_1=\frac{U_1}{(\gamma k_B T_1/m)^{1/2}}, \tag{42}$$

where $m=m_A\chi^A+m_B\chi^B$. The Rankine-Hugoniot condition [48] holds for each species, so the downstream quantities are

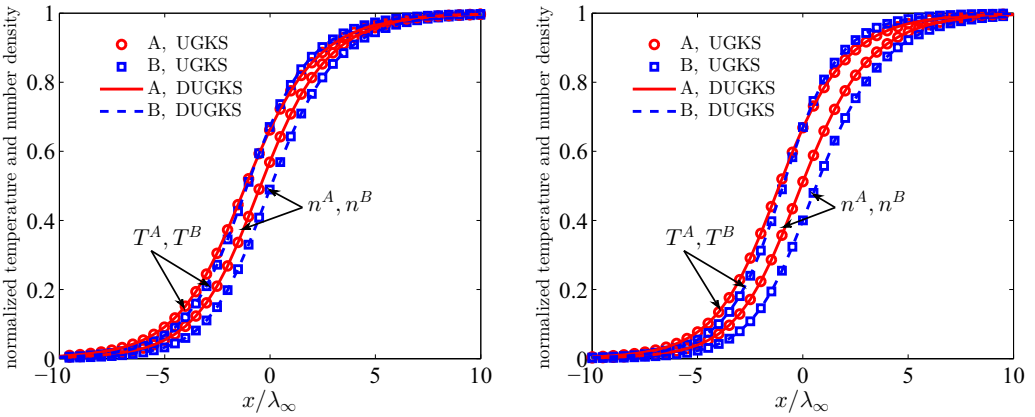

FIG. 1. Structure of a $\mathrm{Ma}_1 = 1.5$ shock wave in a binary gas mixture with $m_A/m_B = 0.5$ and $a_{BB}/a_{AA} = 1$: (a) $\chi_1^A = 0.1$; (b) $\chi_1^A = 0.9$.

then determined as

$$\begin{aligned}
\mathrm{Ma}_2 &= \sqrt{\frac{\mathrm{Ma}_1^2(\gamma-1)+2}{2\gamma\mathrm{Ma}_1^2-(\gamma-1)}},\\
\chi_2^{A,B} &= \chi_1^{A,B},\\
\frac{n_2^A}{n_1^A} &= \frac{n_2^B}{n_1^B} = \frac{(\gamma+1)\mathrm{Ma}_1^2}{(\gamma-1)\mathrm{Ma}_1^2+2},\\
\frac{T_2}{T_1} &= \frac{[2+(\gamma-1)\mathrm{Ma}_1^2](2\gamma\mathrm{Ma}_1^2-\gamma+1)}{\mathrm{Ma}_1^2(\gamma+1)^2}.
\end{aligned} \tag{43}$$

The reference mean free path is defined as [49]

$$\lambda_\infty = \frac{\mu_B}{P_0}\sqrt{\frac{2k_BT_1}{m_B}}, \tag{44}$$

where $P_0 = n_1k_BT_1$ and μ_B is the viscosity of species B defined in Eq. (16). In the simulations, the computation domain is set to be $[-25\lambda_\infty, 25\lambda_\infty]$, which is divided into 100 uniform cells. The velocity space is discretized by Newton-Cotes quadrature with 101 velocity points distributed uniformly in $[-8\sqrt{2k_BT_1/m}, 8\sqrt{2k_BT_1/m}]$. The CFL number is set to be 0.6. The origin of the distribution is determined so that $n(0) = (n_1+n_2)/2$. The simulation results are normalized as

$$\widehat{n}^{A,B} = \frac{n^{A,B}-n_1^{A,B}}{n_2^{A,B}-n_1^{A,B}}, \quad \widehat{T}^{A,B} = \frac{T^{A,B}-T_1^{A,B}}{T_2^{A,B}-T_1^{A,B}}, \tag{45}$$

where the hat will be dropped for simplicity in the following.

The number density and temperature of each species under different Mach numbers and concentrations are shown and compared with those of the UGKS method [28,29] in Figs. 1–3. Good agreement between the two methods can be observed. As shown in Fig. 1 for $\mathrm{Ma}_1 = 1.5$ and $m_A/m_B = 0.5$, the number density n_A and temperature T_A of the light species first deviate from their upstream quantities, and n_A reaches its downstream quantity earlier than n_B. However, the temperature of the heavy species, T_B, arises rapidly, then exceeds that of the light one (T_A), and finally reaches its downstream quantity earlier. These phenomena become more obvious as the concentration of the light species becomes large. Figure 2 presents the results for smaller values of m_A/m_B under $\mathrm{Ma}_1 = 1.5$. It can observed that the above features appear more clearly. The results with $\mathrm{Ma}_1 = 3$ and $m_A/m_B = 0.5$ are shown in Fig. 3, and the above phenomena still exist. However, T_B does not arise monotonically for large concentration of the light species. At the beginning, it approximates the maximum value and then

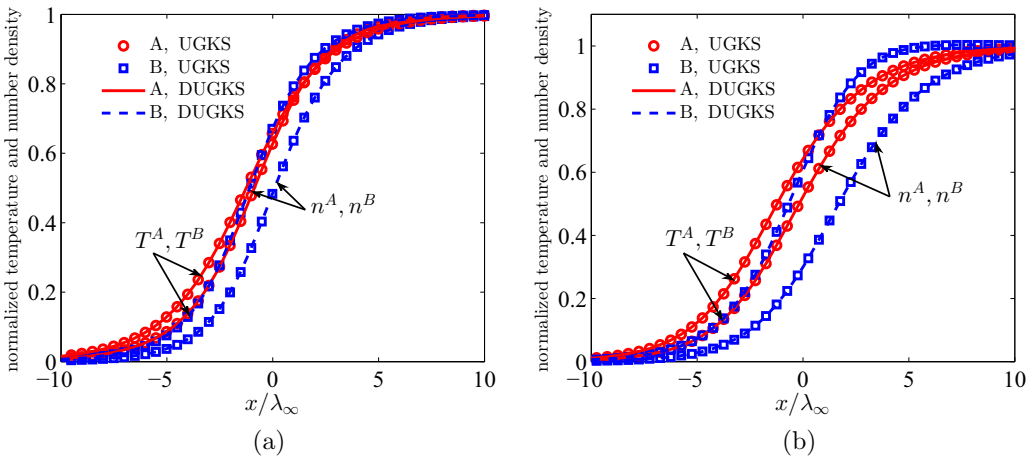

FIG. 2. Structure of a $\mathrm{Ma}_1 = 1.5$ shock wave in a binary gas mixture with $m_A/m_B = 0.25$ and $a_{BB}/a_{AA} = 1$: (a) $\chi_1^A = 0.1$; (b) $\chi_1^A = 0.9$.

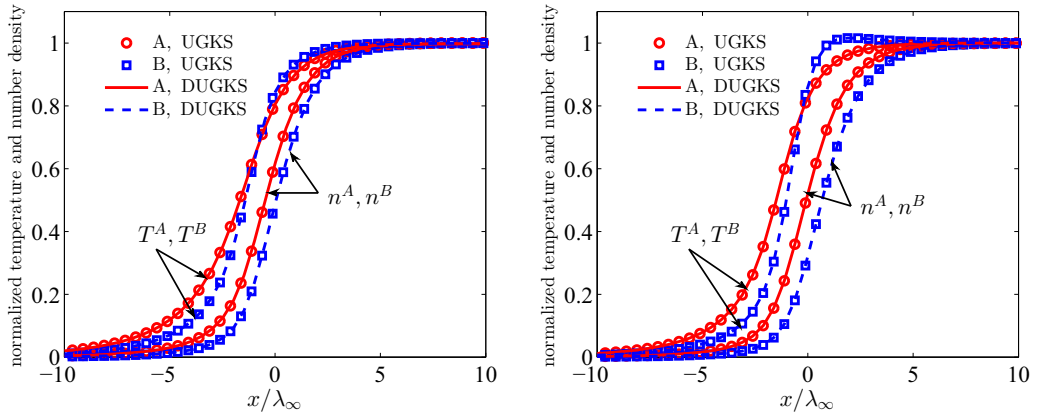

FIG. 3. Structure of a $\mathrm{Ma}_1 = 3.0$ shock wave in a binary gas mixture with $m_A/m_B = 0.5$ and $a_{BB}/a_{AA} = 1$: (a) $\chi_1^A = 0.1$; (b) $\chi_1^A = 0.9$.

decreases to its downstream quantity, which has been known as the temperature overshoot [50].

B. Channel flow driven by a gradient

Now we consider a binary mixture flow in a long channel with width H (see Fig. 4). A uniform pressure gradient, or temperature gradient or concentration gradient, exists along the channel (x direction), i.e., $p = p_0(1 + C_p x/H)$, $T = T_0(1 + C_T x/H)$, $\chi^A = \chi_0^A + C_\chi x/H$, where C_p, C_χ, C_T, p_0, and T_0 are constants. Both plates are fully diffusive and a uniform temperature gradient $T_0(1 + C_T x/H)$ is maintained. The inlet and outlet are imposed with pressure boundary conditions based on characteristics as described in Ref. [28]. In this case, the numerical results are compared with those from Kosuge [51] based on the McCormack model. The definitions of the intermolecular potential and the reference diameter for Maxwell molecules are [51]

$$U_{\alpha\beta} = \frac{\kappa_{\alpha\beta}}{r^4}, \quad d_*^{\alpha\beta} = \left(\frac{4\kappa_{\alpha\beta}}{2k_B T_0}\right)^{\frac{1}{4}}, \tag{46}$$

in which $\kappa_{\alpha\beta}$ is a positive constant. Comparing Eq. (46) with Eq. (14), one can obtain that

$$a_{\alpha\beta} = 4\kappa_{\alpha\beta}; \tag{47}$$

thus the relationship between $d_*^{\alpha\beta}$ and $a_{\alpha\beta}$ is

$$d_*^{\alpha\beta} = \left(\frac{a_{\alpha\beta}}{2k_B T_0}\right)^{\frac{1}{4}}. \tag{48}$$

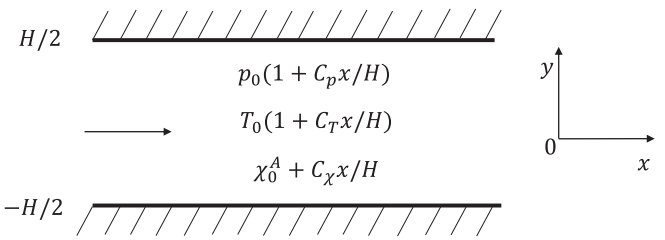

FIG. 4. Schematic of the channel flow.

The reference mean free path is given by [51]

$$\lambda = \frac{1}{\sqrt{2}\pi n_0 (d_*^{AA})^2}, \tag{49}$$

where n_0 is the total number density at the inlet. In the simulations, we consider the flow driven by the pressure gradient, temperature gradient, and concentration gradient separately. For the pressure driven flow, C_T and C_χ are zero and the nondimensional particle flux of each species is defined by [51]

$$M_p^{A,B} = \frac{1}{C_p}\int_{-H/2}^{H/2} \frac{u_{A,B}}{\sqrt{2k_B T_0/m_A}} d(y). \tag{50}$$

The fluxes $M_T^{A,B}$ and $M_\chi^{A,B}$ due to the temperature gradient and concentration gradient can be defined similarly.

In our simulations, the length-to-height ratio of the channel is set to be 40 and the gradient C_p, C_χ, and C_T are kept at 0.01. The particle fluxes versus Knudsen number are displayed in Figs. 5–7 for $m_B/m_A = 2, 4$, and 10 with $a_{BB}/a_{AA} = a_{AB}/a_{AA} = 1$. The results of the UGKS for binary gas mixtures [28,29] of Maxwell molecules are also included for comparison. Overall good agreement between the DUGKS and UGKS can be observed for the cases considered.

In Fig. 5, the mass fluxes driven by a pressure gradient show good agreement with the solutions of the linearized Boltzmann equation [51], with some minor deviations. The differences can be attributed to the discrepancy in viscosity from different models. Furthermore, it can be observed that a minimum appears for each species around $\mathrm{Kn} \approx 1$, which is the well-known Knudsen minimum [52] for Poiseuille flow in rarefied regime.

Figure 6 shows the mass fluxes of each species for flows driven by a temperature gradient. It can be seen that M_T^A and M_T^B increase monotonically with Kn, and their difference decreases with Kn.

Furthermore, it is observed that the predicted mass fluxes of the heavy species B match quite well with the reference solutions. But clear deviations can be observed for the light species A and the deviations increase with Kn. This can be attributed to the different thermal conductivities from the AAP model and the linearized Boltzmann equation [51].

The mass fluxes at different Knudsen numbers driven by a concentration gradient are shown in Fig. 7. It can be seen

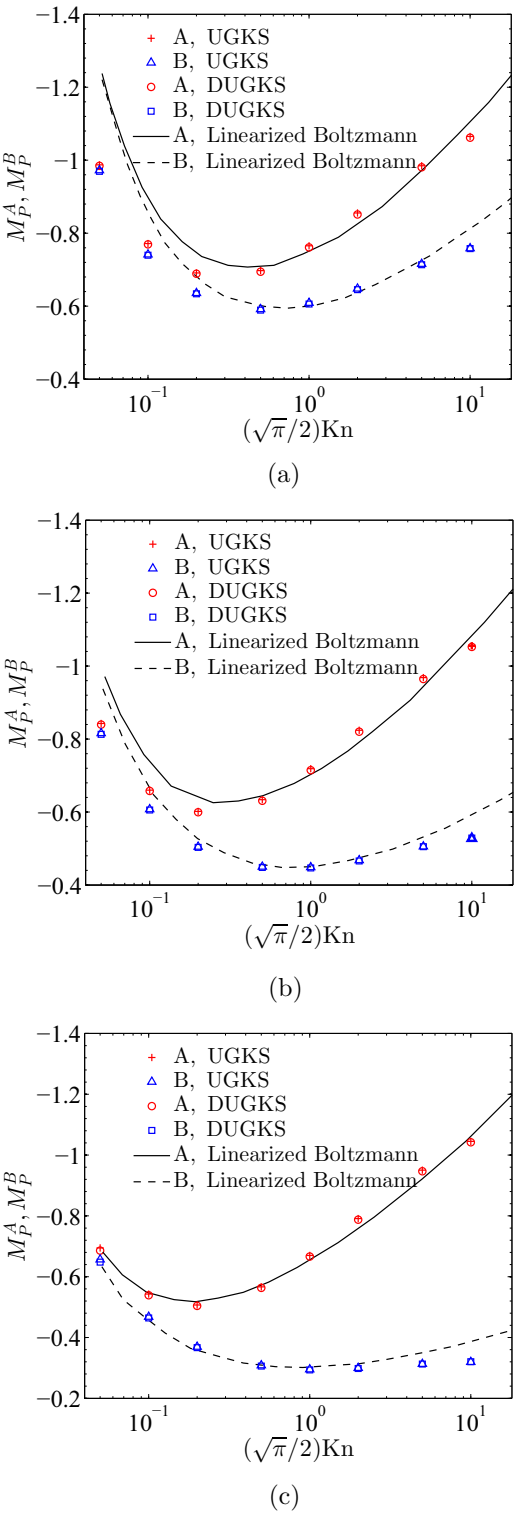

FIG. 5. Particle flux versus Knudsen number of the pressure driven channel flow with $\chi_0^A = 0.5$. m_B/m_A in (a), (b), and (c) is 2, 4, and 10, respectively. The linearized solutions are from Ref. [51].

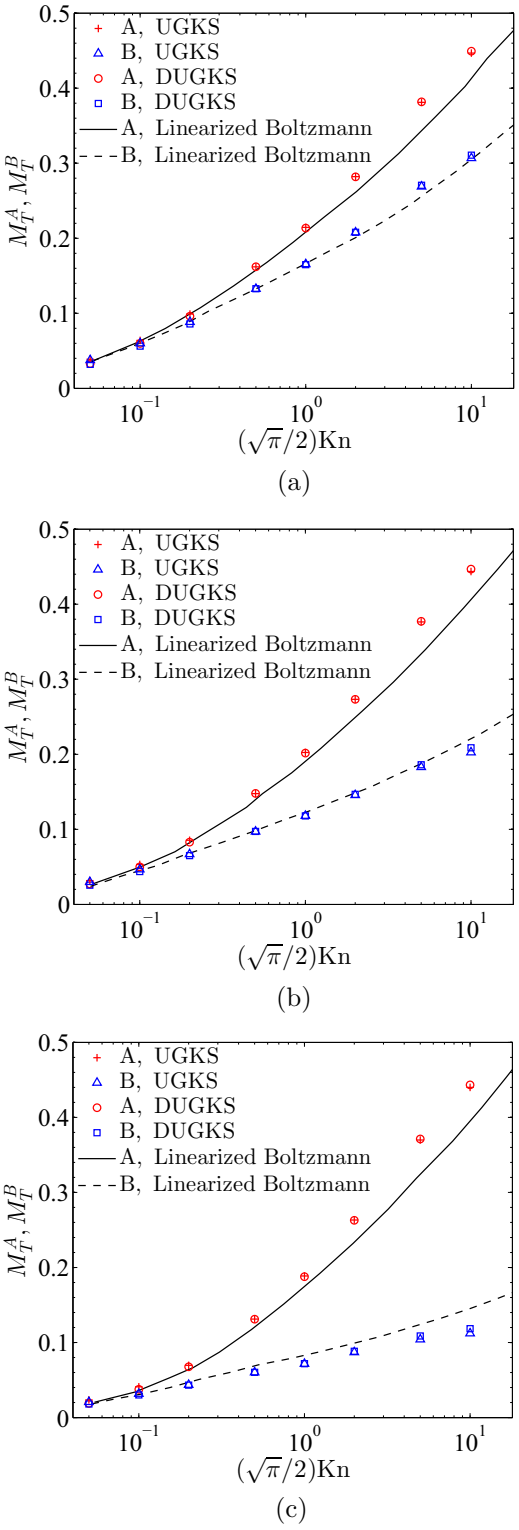

FIG. 6. Same as Fig. 5 except that the flow is driven by a temperature gradient.

that the concentration of the light species A increases while that of the heavy one decreases along the channel. As a result, the light one turns to flow in the opposite direction. But it can be observed that both $|M_\chi^A|$ and M_χ^B grow monotonically with increasing Kn, and the results predicted by the AAP model are in good agreement with the reference data for all cases considered.

It can also be observed that the differences in the mass fluxes of species A and B decrease with increasing Kn driven by the pressure, temperature, or concentration gradient. This is

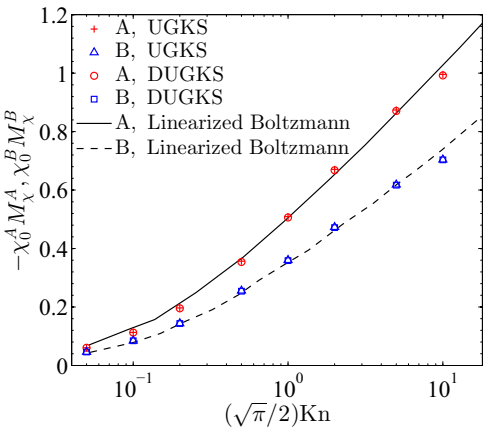

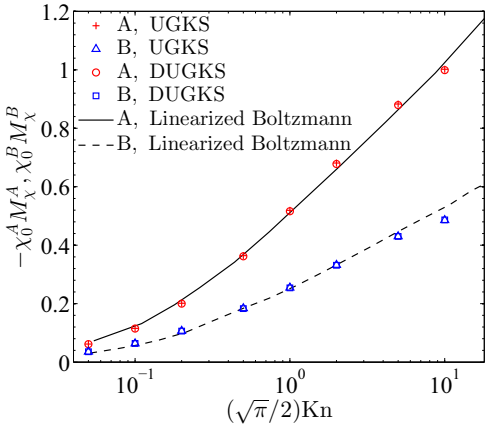

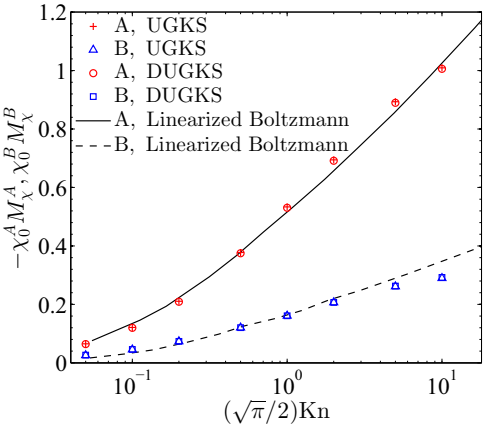

FIG. 7. Same as Fig. 5 except that the flow is driven by a concentration gradient.

because the velocities of the two species are different due to the difference in molecular masses. Particularly, the differences between u_A and u_B can be much larger as the intermolecular collisions are insufficient such that the momentums of the two species are not exchanged sufficiently. On the contrary, the velocities of the two species will become closer in the continuum limit when the collision is frequent.

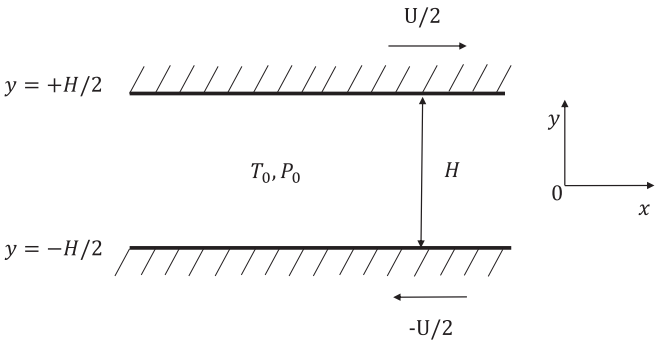

FIG. 8. Schematic of the plane Couette flow.

C. Couette flow

Now we consider the plane Couette flow of a binary gas mixture in the rarefied regime.

As shown in Fig. 8, two plates with a constant temperature T_0 are fixed at $y = \pm H/2$ and move with velocities $\pm U/2$ in the x direction, respectively. The plates are fully diffusive and the periodic boundary conditions are imposed on the inlet and outlet of the channel. Here we assume that the plate velocities are much smaller than the characteristic molecular velocity v_0 of mixture, i.e.,

$$U \ll v_0, \quad v_0 = \sqrt{\frac{2k_B T_0}{m}}, \tag{51}$$

where m is the mean molecular mass of the mixture $m = C_0 m_A + (1 - C_0) m_B$, and C_0 is the molar concentration of the light species in equilibrium,

$$C_0 = \frac{n_A^0}{n_A^0 + n_B^0}, \tag{52}$$

with n_A^0,n_B^0 being the equilibrium number density of species A and B, respectively. In this case, we focus on the shear stress $P'_{xy} = P'_{Axy} + P'_{Bxy}$ of the mixture and the velocity u'_α of species α. The shear stress $P'_{\alpha xy}$ of species α is calculated according to Eq. (22). The velocity of the mixture in the x direction is defined as

$$u_{m,x} = \frac{\rho_A u'_{A,x} + \rho_B u'_{B,x}}{\rho_A + \rho_B}. \tag{53}$$

The gas rarefaction parameter δ is defined as

$$\delta = \frac{H P_0}{\mu v_0}, \quad P_0 = n_0 k_B T_0, \tag{54}$$

where μ is the mixture viscosity at temperature T_0, and P_0 is the equilibrium pressure with n_0 being the total number density of the two species. Then we can get the following dimensionless quantities

$$u_\alpha = \frac{u'_\alpha}{U}, \quad P_{xy} = -\frac{v_0}{2U P_0} P'_{xy}. \tag{55}$$

To calculate a_{BB}/a_{AA} by Eq. (17), the mass ratio and viscosity ratio should be known. Here we consider two groups of binary gas mixtures of noble gases: neon-argon (Ne-Ar) and helium-xenon (He-Xe). The molecular masses of these gases are $m_{\rm He} = 4.0026$, $m_{\rm Ne} = 20.1791$, $m_{\rm Ar} = 39.948$, and $m_{\rm Xe} = 131.293$ in atomic units. The experimental data [53] of

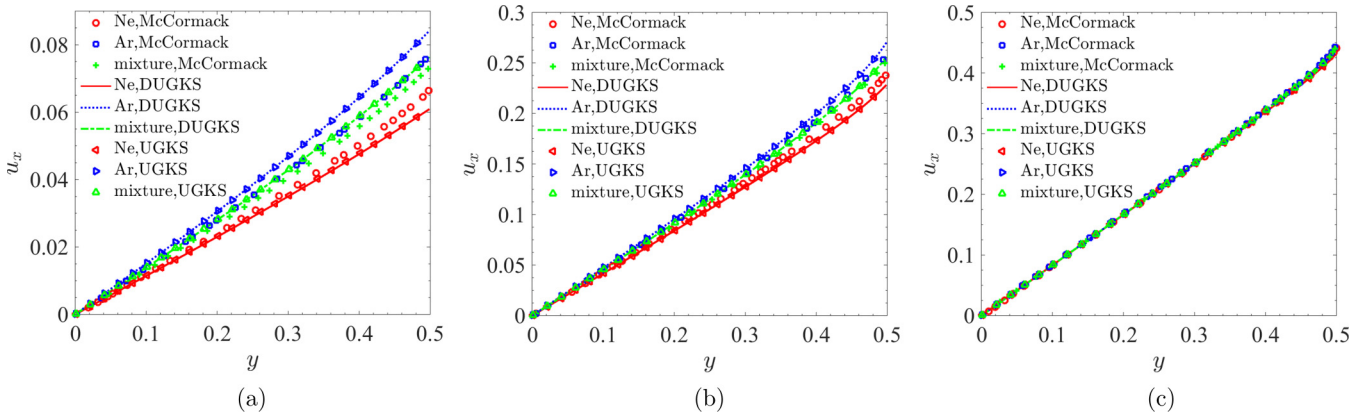

FIG. 9. Velocity profiles in the Couette flow for the Ne-Ar mixture with $C_0 = 0.5$ at (a) $\delta = 0.1$, (b) $\delta = 1$, and (c) $\delta = 10$.

the viscosities at an equilibrium temperature $T_0 = 300$ K are $\mu_{\rm He} = 19.73$ μPa s, $\mu_{\rm Ne} = 31.60$ μPa s, $\mu_{\rm Ar} = 22.39$ μPa s, and $\mu_{\rm Xe} = 22.62$ μPa s.

In our simulations, we take $U = 0.1v_0$ and the rarefaction parameter δ varies from 0.1 to 10. Three values of $C_0 = 0.1$, 0.5, and 0.9 are considered. The physical space is divided uniformly into 2 grid points in the x direction and 400 in the y direction. The half-range Gauss-Hermite quadrature [54] with 28×28 velocity points is adopted for each species. The CFL number is set to be 0.6 in the following cases. In addition, the flow field is assumed to be steady when the maximum relative change of the velocity field of the two species in two successive steps is less than 10^{-10}, i.e.,

$$\int_{-1/2}^{1/2} \max\left(\frac{|u_{A,x}^{n+1} - u_{A,x}^{n}|}{|u_{A,x}^{n}|}, \frac{|u_{B,x}^{n+1} - u_{B,x}^{n}|}{|u_{B,x}^{n}|}\right) dy < 10^{-10}. \tag{56}$$

The results of the present DUGKS will be compared with the solutions of the McCormack model in Refs. [55,56]. The results of the UGKS for binary gas mixtures [28,29] of Maxwell molecules are also presented for comparison. A comparative study between the McCormack model and the linearized Boltzmann equation for this problem was performed in Ref. [56]. The results indicate that differences in shear stress between the two models are small, while differences in other macroscopic quantities such as the velocity of each species are rather large, which increase with the mass ratio of the two species and the molar concentration of the heavy species.

The velocity profiles for the Ne-Ar and He-Xe mixtures with molar concentration $C_0 = 0.5$ at $\delta = 0.1$, 1, and 10 are demonstrated in Fig. 9 and Fig. 10. It can be seen that the results predicted by the DUGKS agree well with those by the UGKS at different rarefaction parameters. As $\delta = 0.1$, the velocity differences of Ne and Ar between the DUGKS and the McCormack model are about 8% and 9%, respectively. As $\delta = 1$, the velocity differences decrease. As $\delta = 10$, there are slightly differences in the velocity of the two species, i.e., 1.5% for Ne and 0.04% for Ar. The velocity of the He-Xe mixture is also shown in Fig. 10 to illustrate the influence of the mass ratio on the velocity. It can be seen that the deviations in velocity between the DUGKS and the McCormack model are significant, especially as δ is small. For instance, the velocity difference of He between the two models reaches 46.8% at $\delta = 0.1$. Furthermore, the DUGKS overestimates the Xe velocity by 32.8% compared with the McCormack model. These differences decrease with increasing δ, reducing to 10.6% for He and 2.97% for Xe as $\delta = 10$.

The influence of the molar concentration C_0 on the gas velocity near the plate is displayed in Table I. When $\delta = 0.1$, the velocity difference of Ne between the two kinetic models decreases from 13.9% to 1.8%, while that for Ar increases from 2% to 17% as C_0 increases from 0.1 to 0.9. As $\delta = 1$, the difference in each velocity is smaller than that for $\delta = 0.1$ for all

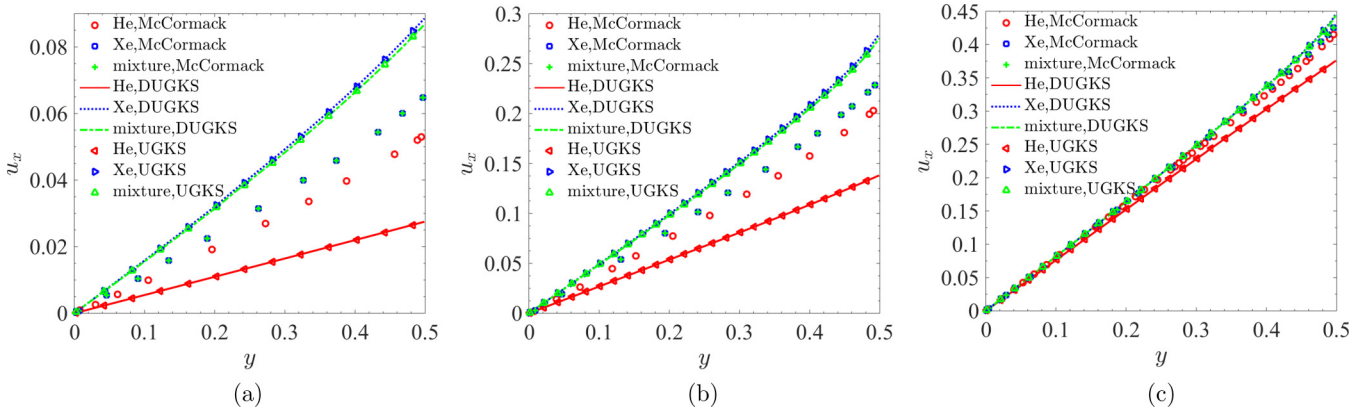

FIG. 10. Same as Fig. 9 but for the He-Xe mixture.

TABLE I. Species velocity u_{Ne} and u_{Ar} and mixture velocity u_m near the top plate ($y = H/2$) for the Ne-Ar mixture with concentration of the light species C_0 and rarefaction parameter δ.

	u_{Ne}			u_{Ar}			u_m		
δ	Present	UGKS	Ref. [56]	Present	UGKS	Ref. [56]	Present	UGKS	Ref. [56]
					$C_0 = 0.1$				
0.1	0.0545	0.0546	0.0633	0.0745	0.0753	0.0736	0.0737	0.0742	0.0730
1.0	0.2141	0.2141	0.2341	0.2542	0.2543	0.2536	0.2521	0.2522	0.2525
10.0	0.4261	0.4261	0.4361	0.4396	0.4397	0.4420	0.4384	0.4389	0.4417
					$C_0 = 0.5$				
0.1	0.0609	0.0610	0.0663	0.0844	0.0842	0.0773	0.0764	0.0764	0.0736
1.0	0.2280	0.2283	0.2399	0.2699	0.2700	0.2598	0.2559	0.2560	0.2531
10.0	0.04310	0.4311	0.4377	0.4437	0.4437	0.4435	0.4394	0.4395	0.4416
					$C_0 = 0.9$				
0.1	0.0699	0.0700	0.0712	0.0973	0.0976	0.0833	0.0749	0.0750	0.0734
1.0	0.2456	0.2457	0.2492	0.2887	0.2889	0.2695	0.2534	0.2535	0.2529
10.0	0.4369	0.4369	0.4407	0.4484	0.4485	0.4463	0.4389	0.4390	0.4417

considered values of C_0. For $\delta = 10$, the velocity difference of Ne between the DUGKS and the McCormack model is less than 2.3% and that of Ar is less than 1% as C_0 varies from 0.1 to 0.9.

The shear stresses P_{xy} of the Ne-Ar and He-Xe mixtures are presented in Table II under different rarefaction parameters and molar concentrations. The shear stress of each mixture should be constant theoretically due to the momentum conservation of the mixture, while the numerical results can slightly deviate from the theoretical values. Thus the average shear stress $P_{xy}^{av} = \int_{-H/2}^{H/2} P_{xy}(y)dy$ is presented here. The maximum variation of the shear stress is calculated as

$$\Delta P_{xy} = \max_{y\in[-\frac{H}{2},\frac{H}{2}]} \left\| \frac{P_{xy}(y) - P_{xy}^{av}}{P_{xy}^{av}} \right\|, \tag{57}$$

which is less than 0.7% according to Eq. (57), showing a good numerical accuracy of the proposed DUGKS. In the Ne-Ar mixture, the differences in shear stress between the results obtained from the DUGKS and the McCormack model are less than 1% for all values of the considered molar concentration C_0 and rarefaction δ, meaning a good agreement between these two kinetic models at small mass ratio. In the He-Xe mixture whose mass ratio is much greater than that of the Ne-Ar mixture, the relative differences between results from the two kinetic models are less than 1% for all considered values of C_0 at $\delta = 0.01$ and 40. However, the DUGKS underpredicts the shear stress by 2.4% at $C_0 = 0.5$ and 5.6% at $C_0 = 0.9$ when $\delta = 0.1$ for the He-Xe mixture. At $\delta = 1$, the differences increase and reach to 9.7% for $C_0 = 0.5$ and 13.8% for $C_0 = 0.9$. For $\delta = 10$, the differences in shear stress are 8.9% and 6.5% for $C_0 = 0.5$ and $C_0 = 0.9$, respectively. These comparisons indicate that the relative difference in shear stress of the He-Xe mixture between the DUGKS and the McCormack model is much higher than that of the Ne-Ar mixture, especially for $\delta = 1$, at which the difference reaches the maximum.

The influence of the rarefaction parameter δ on the shear stress is demonstrated in Fig. 11 with δ ranging from 0.01 to 80 and $C_0 = 0.5$ for the Ne-Ar and He-Xe mixtures. This shows good agreement between the DUGKS and the McCormack model over the whole range of the flow regime for the Ne-Ar mixture, while for the He-Xe mixture, clear deviations are observed in the slip and transitional regimes between the two models, suggesting that the difference between the two models increases with mass ratio.

D. Lid driven cavity flow

The last test case is the two-dimensional lid driven cavity flow of binary gas mixtures. The flow domain is a square

TABLE II. The shear stresses in the Couette flow of the Ne-Ar and He-Xe mixtures under different rarefaction parameter δ and concentration of the light species C_0.

	$C_0 = 0.1$			$C_0 = 0.5$			$C_0 = 0.9$		
δ	Present	UGKS	Ref. [55]	Present	UGKS	Ref. [55]	Present	UGKS	Ref. [55]
					Ne-Ar				
0.1	0.2600	0.2600	0.2601	0.2568	0.2568	0.2576	0.2590	0.2590	0.2594
1.0	0.1683	0.1684	0.1689	0.1657	0.1658	0.1675	0.1677	0.1678	0.1685
10.0	0.04143	0.04145	0.04150	0.04115	0.04112	0.04139	0.04137	0.04142	0.04147
					He-Xe				
0.1	0.2522	0.2523	0.2527	0.2111	0.2112	0.2163	0.1810	0.1811	0.1919
1.0	0.1641	0.1642	0.1655	0.1337	0.1338	0.1482	0.1171	0.1171	0.1360
10.0	0.04094	0.0410	0.04128	0.03645	0.03646	0.03999	0.03642	0.03643	0.03898

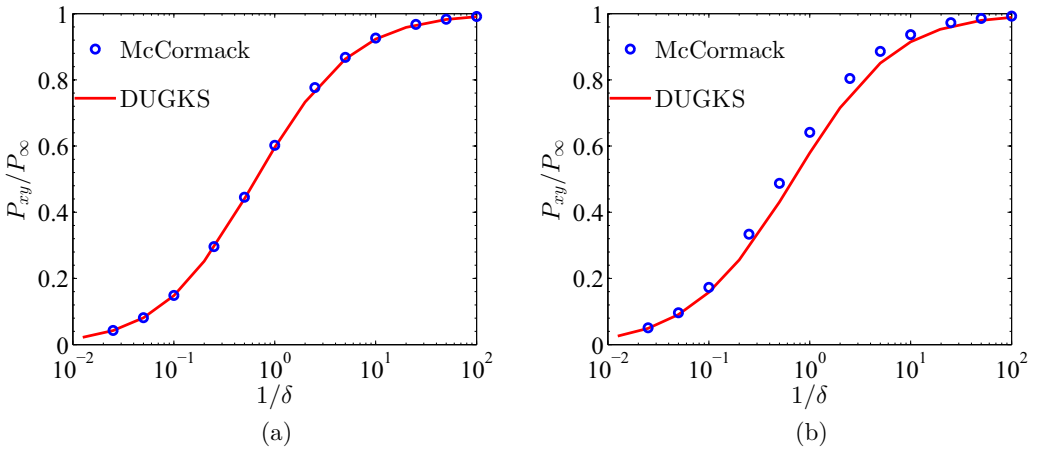

FIG. 11. The normalized stress of the Couette flow for gas mixtures (a) Ne-Ar and (b) He-Xe under different rarefaction parameters δ with $C_0 = 0.5$.

cavity with length H and the upper wall moves with a constant velocity U_w which is also much smaller than the characteristic molecular velocity v_0 in Eq. (51), while other walls are fixed. The temperature at the four walls is fixed at T_0, and the walls are fully diffusive. The Ne-Ar and He-Xe mixtures are considered to investigate the influence of the mass ratio on the mixture velocity and temperature. We also simulate this problem by the UGKS [28,29] and the DSMC [57] to validate the current DUGKS method.

First, to verify the indifferentiability principle of the AAP model, we set $m_A/m_B = 1$, $\mu_A/\mu_B = 1$, and $a_{AA}/a_{BB} = 1$; namely, the mixture reduces to a single-species gas. The rarefaction parameter δ is related to the Reynolds number as

$$\delta = \frac{\mathrm{Re} k_B T_0}{m_A U_w v_0}, \tag{58}$$

where

$$\mathrm{Re} = \frac{\rho_0 U_w H}{\mu_A}, \quad \rho_0 = n_0 m_A. \tag{59}$$

In the simulations, we take $U_w = 0.1 v_0$. The velocity space is discretized via the half-range Gauss-Hermite quadrature with 8×8 velocity nodes. The physical space is divided into 120×120 uniform cells. The CFL number is set to be 0.6. Figure 12 shows the velocity profiles along the center lines of the cavity at $\mathrm{Re} = 400$. The Ghia benchmark solutions [58] are also included for comparison. It can be seen that the DUGKS results agree well with the benchmark data, suggesting that the AAP model satisfies the indifferentiability principle, which requires that the total distribution function $f = \sum_{\alpha=A,B} f_\alpha$ satisfies the single-species BGK equation when the two species are the same. Besides, the ratio of the time step to the mean collision time ($\Delta t/\tau$) is about 3.146 for this case ($\mathrm{Kn} \approx 5 \times 10^{-4}$), which clearly shows that the time step of the DUGKS is not limited by the mean collision time. Thus the AP property of the DUGKS for the Navier-Stokes limit is validated.

Then the flows of two groups of binary gas mixtures (Ne-Ar and He-Xe) are simulated. The velocity space for each species is discretized using the Newton-Cotes rule, with 101×101 velocity points distributed uniformly in $[-4\sqrt{2R_\alpha T_0}, 4\sqrt{2R_\alpha T_0}] \times [-4\sqrt{2R_\alpha T_0}, 4\sqrt{2R_\alpha T_0}]$. The physical space is divided into 60×60 cells uniformly, where the results are nearly identical to those on a 100×100 mesh.

The velocity profiles of the two mixtures across the cavity center for $\delta = 0.1$, 1, and 10 under the concentration of the light species $C_0 = 0.5$ are presented in Figs. 13 and 14. Good agreement can be observed between the DUGKS and the UGKS and DSMC results for the Ne-Ar mixture as δ varies from 0.1 to 10. However, for the He-Xe mixture, whose molecular mass ratio is large, deviations between the solutions of DSMC and the DUGKS increase with δ. This discrepancy can be attributed to the relaxation approximation of the collision operator. The above comparisons show that the DUGKS based on the AAP model can offer accurate flow solutions for flows in the rarefied regimes, as the molecular mass ratio is not large.

Similar phenomena can also be found in the temperature field as shown in Figs. 15 and 16. The translational kinetic

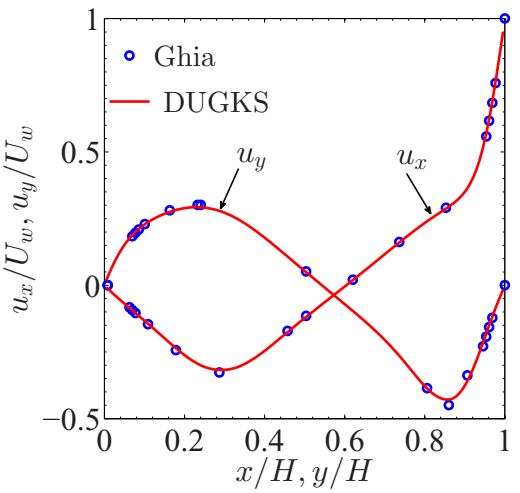

FIG. 12. Velocity profiles across the cavity center at $\mathrm{Re} = 400$.

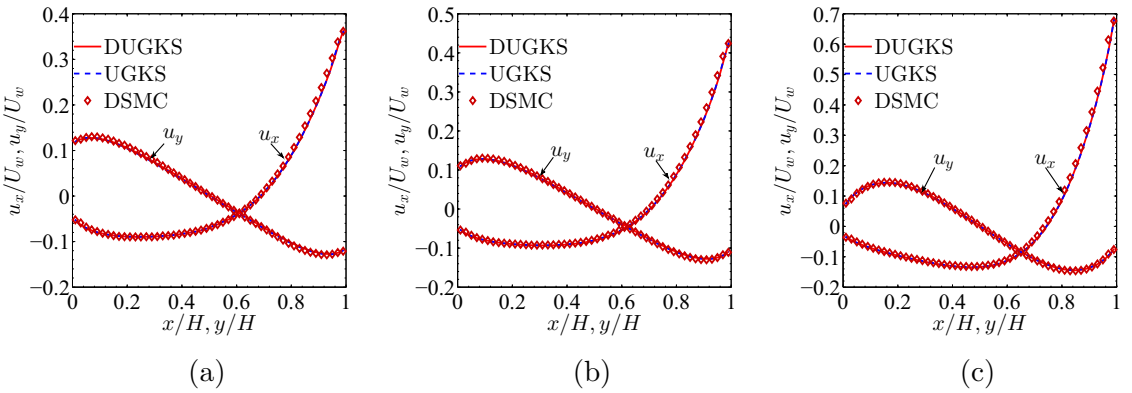

FIG. 13. Velocity profiles along the center lines in the cavity flow for the Ne-Ar mixture with $C_0 = 0.5$ at (a) $\delta = 0.1$, (b) $\delta = 1$, and (c) $\delta = 10$.

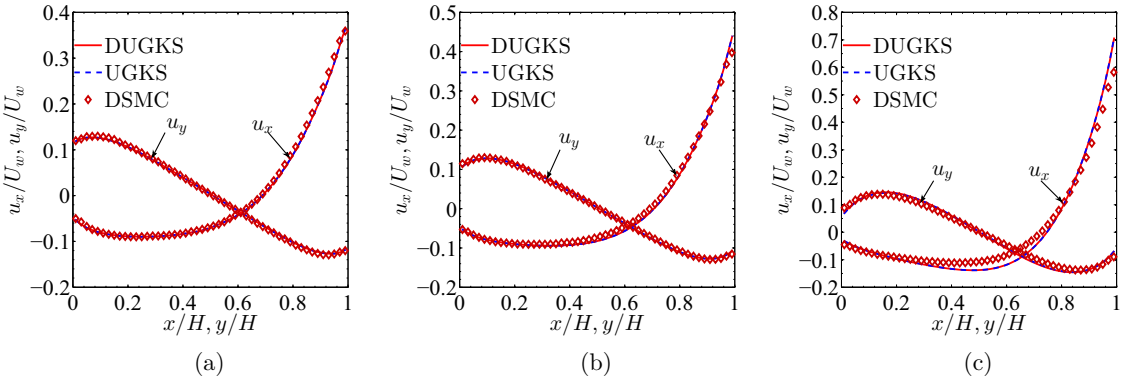

FIG. 14. Same as Fig. 13 but for the He-Xe mixture.

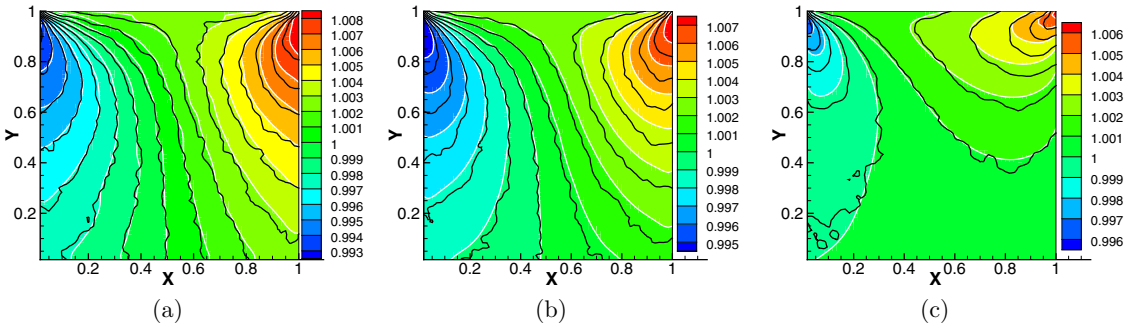

FIG. 15. Temperature contours in the lid driven cavity flow for the Ne-Ar mixture with $C_0 = 0.5$ at (a) $\delta = 0.1$, (b) $\delta = 1$, and (c) $\delta = 10$. Black line: DSMC; white line with background: DUGKS.

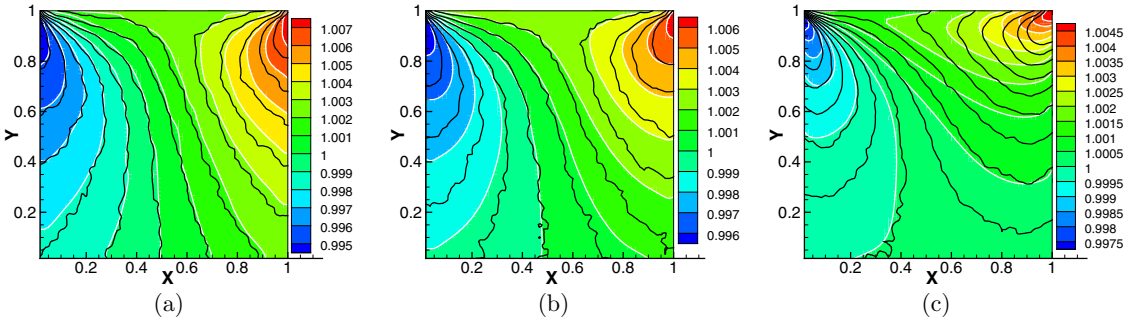

FIG. 16. Same as Fig. 15 but for the He-Xe mixture.

TABLE III. Wall time (in seconds) and iteration steps of reaching steady states. 24 cores are used in the DUGKS and UGKS, and 48 cores are used in DSMC.

δ	DUGKS		UGKS		DSMC	
	time	step	time	step	time	step
0.1	11454	17217	18787	19880	37534	6 110 000
1	7240	9625	8314	8770	58244	10 000 000
10	10470	14516	15633	16490	92043	10 000 000

temperature [6] is considered in this case, which is defined by

$$\frac{3}{2}k_B T_{\rm tr} = \frac{1}{2}\sum_{\alpha}(n_\alpha/n)m_\alpha\overline{c_\alpha'^2}, \tag{60}$$

where $\overline{c_\alpha'^2}$ can be expressed as

$$\overline{c_\alpha'^2} = u_\alpha^2 + 3R_\alpha T_\alpha - u_m^2. \tag{61}$$

For the Ne-Ar mixture with a small mass ratio, the DUGKS results agree excellently with the DSMC solutions in all cases. For the He-Xe mixture with a large mass ratio, the results of DUGKS and UGKS always have good agreement, while they deviate from the DSMC solutions for large δ.

In order to evaluate the computational efficiency, we also measure the computing time of the DUGKS, UGKS, and the DSMC method using the lid driven cavity flow case with the Ne-Ar mixture. Both the DUGKS and UGKS are run with 24 cores using OpenMP programming, while the DSMC solver is run with 48 cores using MPI programming. The wall time (in seconds) and numbers of iterations to reach the steady states in DUGKS/UGKS and the current noise level in DSMC for $\delta = 0.1$, 1, and 10 are listed in Table III. We can see the DUGKS is about 15% to 64% faster than UGKS depending on the rarefaction degree and is significantly faster than the DSMC method.

V. CONCLUSIONS

In this paper, a DUGKS is developed for flows of binary gas mixtures of Maxwell molecules in the whole range of the Knudsen number based on the AAP model. The numerical scheme possesses the asymptotic preserving (AP) property, which means that the time step and the cell size are not constrained by the particle collision time and the mean free path of gas molecules, respectively, when solving the Navier-stokes equations at the continuum limit.

In order to validate the DUGKS, several tests have been performed, including the shock structure, the channel flows driven by a small gradient of pressure, or temperature, or concentration, the plane Couette flow, and the cavity flow in all flow regimes. Excellent agreement has been obtained between the solutions of the DUGKS and the UGKS for all cases, and good agreement with the reference solutions is obtained at moderate Knudsen numbers and mass ratios in channel flow, especially for the heavy species. But some deviations in temperature are found for the light species, which can be attributed to the incorrect Prandt number of the AAP model. For the plane Couette flow, the DUGKS results agree well with those of the McCormack model at small mass ratio and small Knudsen numbers; otherwise obvious differences are observed. As for the cavity flow, the proposed DUGKS results agree well with the DSMC solutions in all flow regimes when the mass ratio is small, but clear deviations appear in the near-continuum regime with large mass ratio, which can be attributed to the relaxation approximation of the collision operator.

Finally, it should be pointed out that the present DUGKS is based on the AAP model for Maxwell molecular gases, which has its own limitations as indicated in the simulation results. Further development of the method based on more accurate kinetic models such as the ellipsoidal models [59,60] or the McCormack model will be studied in future work.

ACKNOWLEDGMENTS

This study is financially supported by the National Key Research and Development Plan (No. 2016YFB0600805) and the National Natural Science Foundation of China (No. 11702223).

[1] F. Sharipov, *Rarefied Gas Dynamics: Fundamentals for Research and Practice* (John Wiley & Sons, New Jersey, 2015).
[2] G. Karniadakis, A. Beskok, and M. Gad-El-Hak, Appl. Mech. Rev. **55**, B76 (2002).
[3] O. Aktas, N. Aluru, and U. Ravaioli, J. Microelectromech. Syst. **10**, 538 (2001).
[4] F. Sharipov and J. L. Strapasson, Phys. Fluids **25**, 027101 (2013).
[5] L. Szalmas, D. Valougeorgis, and S. Colin, in *Proceedings of ASME 2011 9th International Conference on Nanochannels, Microchannels, and Minichannels* (ASME, Edmonton, Alberta, Canada, 2011), Vol. 1, pp. 279–288.
[6] G. A. Bird, *Molecular Gas Dynamics and the Direct Simulation of Gas Flows* (Clarendon Press, Cotswolds, 1994).
[7] T. M. Homolle and N. G. Hadjiconstantinou, J. Comput. Phys. **226**, 2341 (2007).
[8] L. Szalmas, J. Comput. Phys. **231**, 3723 (2012).
[9] S. Kosuge, K. Aoki, and S. Takata, Eur. J. Mech. B/Fluids **20**, 87 (2001).
[10] S. Kosuge, K. Aoki, and S. Takata, AIP Conf. Proc. **585**, 289 (2001).
[11] R. Garcia and C. Siewert, Eur. J. Mech. B/Fluids **26**, 749 (2007).
[12] R. Garcia and C. Siewert, Eur. J. Mech. B/Fluids **27**, 823 (2008).
[13] F. J. McCormack, Phys. Fluids **16**, 2095 (1973).
[14] S. Kosuge, Eur. J. Mech. B/Fluids **28**, 170 (2009).
[15] C. Tantos and D. Valougeorgis, Int. J. Heat Mass Transf. **117**, 846 (2018).
[16] P. Andries, K. Aoki, and B. Perthame, J. Stat. Phys. **106**, 993 (2002).
[17] P. L. Bhatnagar, E. P. Gross, and M. Krook, Phys. Rev. **94**, 511 (1954).
[18] M. Groppi and G. Spiga, Phys. Fluids **16**, 4273 (2004).

[19] M. Groppi, K. Aoki, G. Spiga, and V. Tritsch, Phys. Fluids **20**, 117103 (2008).
[20] C. Liu and K. Xu, Commun. Comput. Phys. **22**, 1175 (2017).
[21] M. Bisi and S. Lorenzani, Phys. Fluids **28**, 052003 (2016).
[22] L. Szalmas, Open Physics **6**, 786 (2008).
[23] P. Asinari and L.-S. Luo, J. Comput. Phys. **227**, 3878 (2008).
[24] Z. Guo, P. Asinari, and C. Zheng, Phys. Rev. E **79**, 026702 (2009).
[25] F. Sharipov and D. Kalempa, J. Vac. Sci. Technol. A **20**, 814 (2002).
[26] S. Naris, D. Valougeorgis, F. Sharipov, and D. Kalempa, Superlattices Microstruct. **35**, 629 (2004).
[27] D. Valougeorgis and S. Naris, SIAM J. Sci. Comput. **25**, 534 (2003).
[28] R. Wang, Unified gas-kinetic scheme for the study of non-equilibrium flows, Ph.D. thesis, Hong Kong University of Science and Technology, 2015 .
[29] R. Wang and K. Xu, AIP Conf. Proc. **1628**, 970 (2014).
[30] K. Xu and J.-C. Huang, J. Comput. Phys. **229**, 7747 (2010).
[31] J.-C. Huang, K. Xu, and P. Yu, Commun. Comput. Phys. **12**, 662 (2012).
[32] L. Mieussens, J. Comput. Phys. **253**, 138 (2013).
[33] Z. Guo, K. Xu, and R. Wang, Phys. Rev. E **88**, 033305 (2013).
[34] Z. Guo, R. Wang, and K. Xu, Phys. Rev. E **91**, 033313 (2015).
[35] P. Wang, L. Zhu, Z. Guo, and K. Xu, Commun. Comput. Phys. **17**, 657 (2015).
[36] P. Wang, S. Tao, and Z. Guo, Computers & Fluids **120**, 70 (2015).
[37] L. Zhu, Z. Guo, and K. Xu, Computers & Fluids **127**, 211 (2016).
[38] L. Zhu and Z. Guo, Phys. Rev. E **95**, 023113 (2017).
[39] Z. Guo and K. Xu, Int. J. Heat Mass Transf. **102**, 944 (2016).
[40] C. Zhang, K. Yang, and Z. Guo, arXiv:1802.02868.
[41] M. Icardi, G. Boccardo, D. L. Marchisio, T. Tosco, and R. Sethi, Phys. Rev. E **90**, 013032 (2014).
[42] T. W. Willingham, C. J. Werth, and A. J. Valocchi, Environ. Sci. Technol. **42**, 3185 (2008).
[43] G. M. Kremer, *An Introduction to the Boltzmann Equation and Transport Processes in Gases* (Springer Science & Business Media, Berlin, Germany, 2010).
[44] T. Morse, Phys. Fluids **6**, 1420 (1963).
[45] J. Yang and J. Huang, J. Comput. Phys. **120**, 323 (1995).
[46] C. K. Chu, Phys. Fluids **8**, 12 (1964).
[47] B. Van Leer, J. Comput. Phys. **23**, 276 (1977).
[48] S. Harris, *An Introduction to the Theory of the Boltzmann Equation* (Courier Corporation, Massachusetts, 2004).
[49] C. Cercignani, *Mathematical Methods in Kinetic Theory* (Springer, Berlin, Germany, 1969).
[50] G. Bird, J. Fluid Mech. **31**, 657 (1968).
[51] S. Kosuge and S. Takata, Eur. J. Mech. B/Fluids **27**, 444 (2008).
[52] C. Cercignani, in *The Boltzmann Equation and Its Applications* (Springer, Berlin, Germany, 1988), pp. 40–103.
[53] J. Kestin, K. Knierim, E. Mason, B. Najafi, S. Ro, and M. Waldman, J. Phys. Chem. Ref. Data **13**, 229 (1984).
[54] B. Shizgal, J. Comput. Phys. **41**, 309 (1981).
[55] F. Sharipov, L. M. G. Cumin, and D. Kalempa, Eur. J. Mech. B/Fluids **23**, 899 (2004).
[56] M. T. Ho, L. Wu, I. Graur, Y. Zhang, and J. M. Reese, Int. J. Heat Mass Transf. **96**, 29 (2016).
[57] T. Scanlon, E. Roohi, C. White, M. Darbandi, and J. Reese, Computers & Fluids **39**, 2078 (2010).
[58] U. Ghia, K. N. Ghia, and C. Shin, J. Comput. Phys. **48**, 387 (1982).
[59] M. Groppi, S. Monica, and G. Spiga, Europhys. Lett. **96**, 64002 (2011).
[60] S. Brull, V. Pavan, and J. Schneider, Eur. J. Mech. B/Fluids **33**, 74 (2012).